Deep states associated with platinum in silicon: A photoluminescence study

G. Armelles, J. Barrau, and M. Brousseau
Laboratoire de Physique des Solides, Institut National des Sciences Appliquées, Avenue de Rangueil, 31077 Toulouse Cedex, France

J. P. Noguier
Le Silicium, Semiconducteur, Usine de Tours, Rue Marie et Pierre Curie, B.P. 0155, 37001 Tours Cedex, France
(Received 3 June 1985)

In this paper we present a photoluminescence study of Si:Pt. Two centers were detected. Piezospectroscopy and Zeeman experiments of one center were carried out. The experiment is well interpreted in terms of a $\Gamma_3+\Gamma_4+\Gamma_5\rightarrow\Gamma_1$ transition in T_d symmetry. The transition is related to the donor center of Pt in silicon at $E_v+0.32$ eV.

I. INTRODUCTION

Platinum is usually diffused in silicon to control the carrier lifetimes. Two levels in the gap are well identified, an acceptor at $E_c-0.23$ eV and a donor at $E_v+0.32$ eV.[1] ESR studies of platinum in silicon were presented some years ago by Woodbury and Ludwing,[2] and more recently by Henning and Egelmeers.[3] One of these ESR signals was attributed to the acceptor center. However, to our knowledge, no photoluminescence (PL) study has been yet carried out on this impurity. In this paper we present such a study.

Two spectra characteristic of Si-diffused samples have been identified and attributed to two distinct defects. One spectrum has a no-phonon transition at 805 meV, and the other a no-phonon structure at 810 meV. Piezospectroscopy and Zeeman experiments were done on one spectrum (805 meV). The study indicates a T_d site symmetry for this center, and a suggestion of its nature is made.

II. EXPERIMENTAL DETAILS

The starting materials were float-zoned (FZ) or Czochralski n-type silicon. A layer of 600 Å of platinum was deposed on the silicon wafers, and the diffusions were carried out at 850 °C, 950 °C, 1050 °C, or 1150 °C for 16 h.

The PL spectra were obtained using a double 0.85-m Spex monochromator and a cooled germanium photodetector. Magnetic fields up to 7 T were generated using a split-coil superconducting magnet, and the experiment was carried out in the Voigt configuration. The samples used in the stress experiments were parallelipiped, and the typical dimensions were $18\times2\times1$ mm^3.

The luminescence was excited by the 752-nm krypton laser line or the 1.06-μm YAG laser (YAG denotes yttrium aluminum garnet) line, the latter excitation was the more efficacious.

III. LUMINESCENCE AS A FUNCTION OF THE TEMPERATURE OF DIFFUSION

We have not observed any specific spectrum in the 850 °C and 950 °C diffused samples. However, the 1050 °C diffused samples show the spectrum presented in Fig. 1. This spectrum consists of only one no-phonon transition at 805.36 meV, labeled B, and some localized replicas at 789 and 776.3 meV. As the sample temperature increases, the intensity of the no-phonon line grows, reaching a maximum at 14 K and then it begins to decrease. This hot line behavior suggests the existence of another excited level at lower energy.

In Fig. 2 we present the spectrum of the 1150 °C dif-

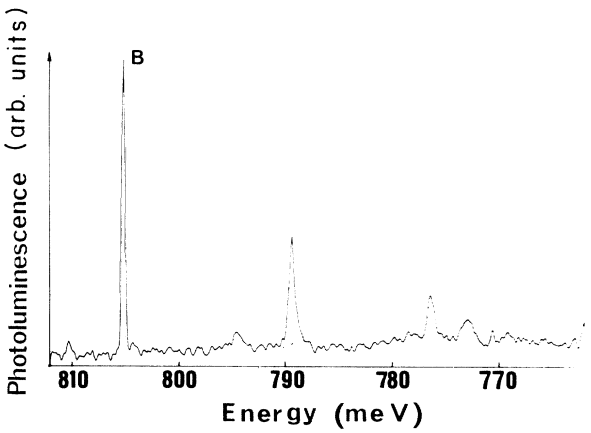

FIG. 1. Luminescence spectrum of the Si:Pt 1050 °C diffused sample.

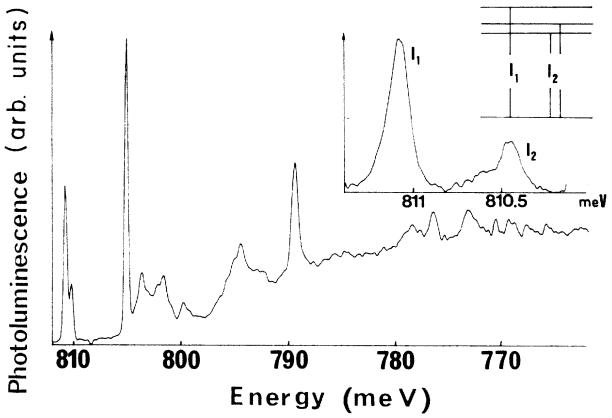

FIG. 2. Luminescence spectrum of the Si:Pt 1150 °C diffused sample. In the inset the spectrum of the no-phonon transition at 810 meV.

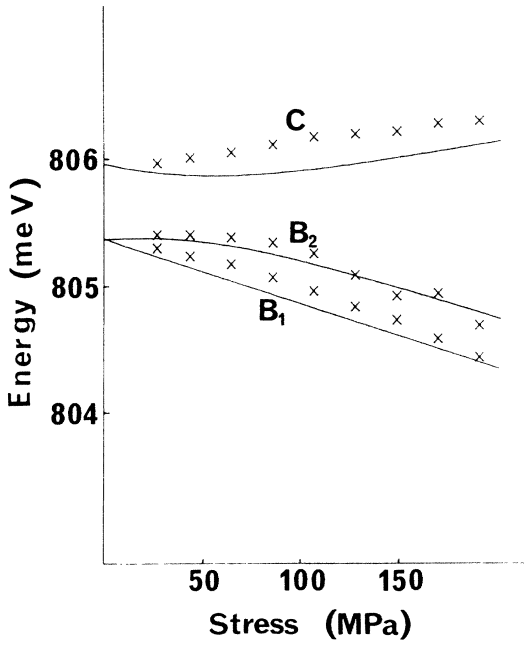

FIG. 3. Fan chart for [001] stress. The solid curves represent the theoretical positions of the dipole-allowed transitions, with the values of A and B given in the text.

fused sample. A new structure appears, co-existing with the preceding transition. This new superimposed spectrum has a no-phonon structure with two lines peaking at 811.08 and 810.45 meV. In the inset of Fig. 2 we present a spectrum of this new set of no-phonon lines with a proposed level scheme. These lines involve a defect distinct from the one investigated, and are not the main subject of the paper.

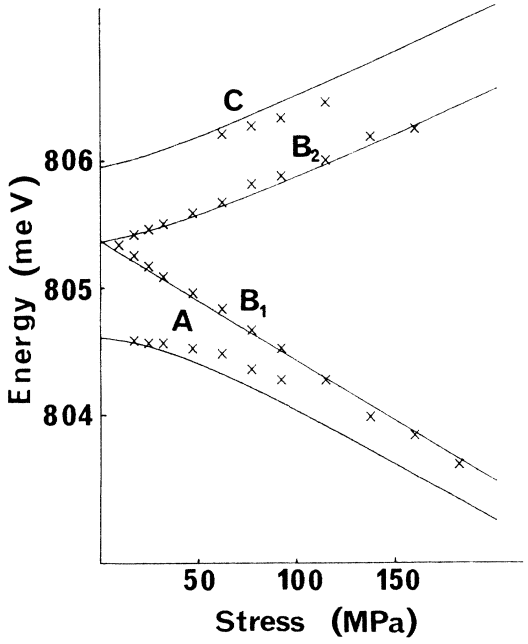

FIG. 4. Fan chart for [111] stress. The curves represent the theoretical positions of the dipole-allowed transitions, with the values of A and C given in the text.

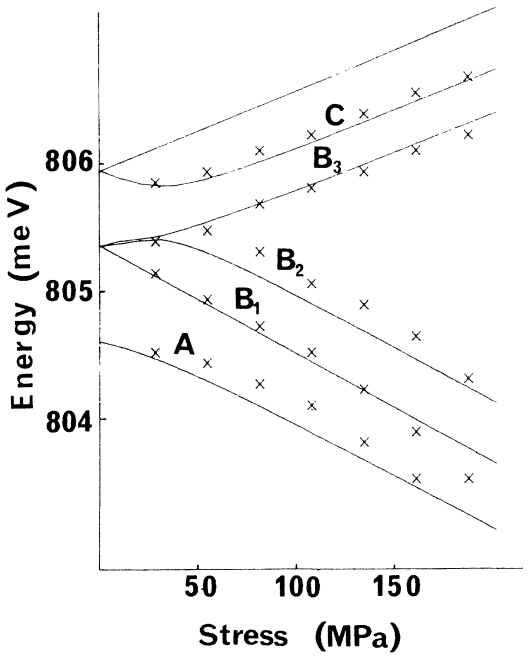

FIG. 5. Development of the stress splitting for P||[110]. The solid curves represent a fit based on Eq. (1) with the values of A, B, and C given in the text.

IV. EXPERIMENTAL STUDY

A. Piezospectroscopic experiment of the 0.805-eV transition

In Figs. 3, 4, and 5, we present the results of the piezospectroscopic experiment relative to the 0.805 eV no-

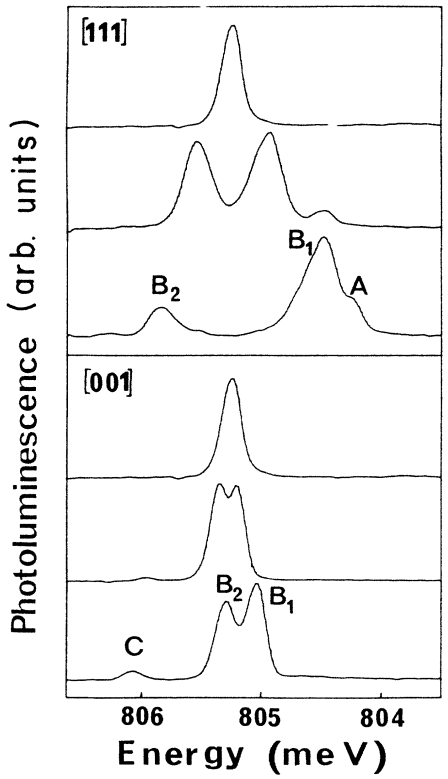

FIG. 6. P||[001] and P||[111], some spectra at different stress intensities.

phonon line. The experimental positions of the lines were obtained from spectra such as those of Fig. 6.

1. P||[001]

For weak stress the B line splits into two components, labeled B_1 and B_2. As the stress increases a new line appears at higher energy, labeled C. The B_1 line is polarized parallel to [001], whereas the C and B_2 lines are polarized perpendicular to [001].

2. P||[111]

The B line splits into two components labeled B_1 and B_2. As the stress increases a new line appears at lower energy, labeled A, and reaches the B_1 line at high stress. The B_2 and A lines are polarized perpendicular to [111], whereas the B_1 line is polarized parallel to [111]. The C line is also seen but with weak intensity, and its polarization is hard to determine.

3. P||[110]

In this direction the C and A lines appear as the stress increases. The B line splits into three components, labeled B_1, B_2, B_3. The B_1 line is polarized parallel to [110], the others (A, B_2, B_3) are polarized perpendicular to [110]. A common feature for the three directions is that all lines remain thermalized together.

B. Zeeman experiment

In Fig. 7, some spectra are shown at a field intensity of 3 or 6 T for **H** parallel to [001], [111], or [110].

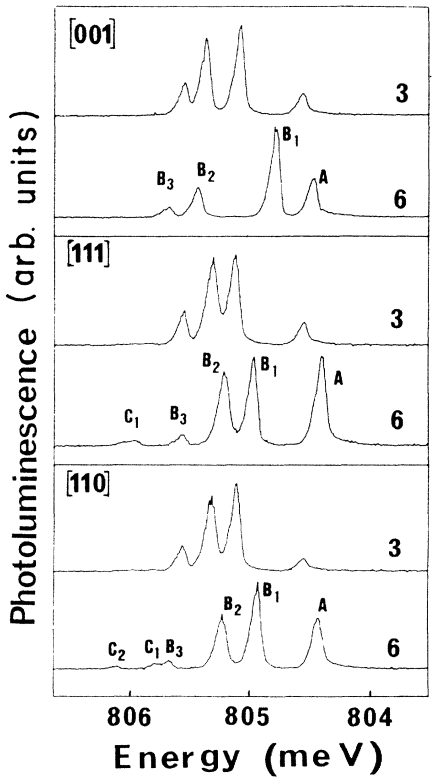

FIG. 7. Zeeman spectra for a field intensity of 3 or 6 T.

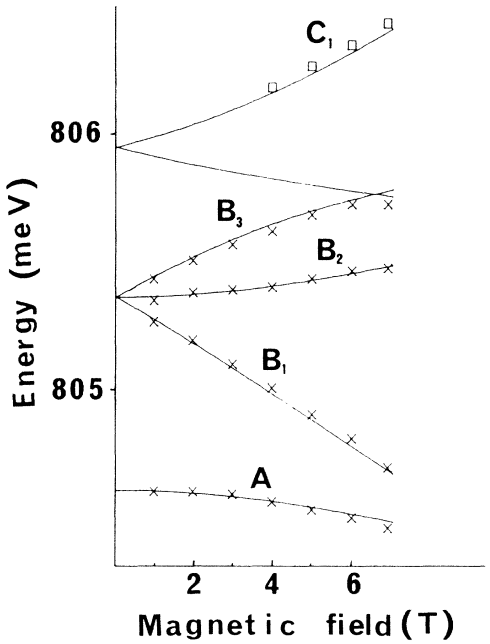

FIG. 8. Development of the Zeeman splitting for H||[001]. The solid curves are a fit based on Eq. (2). □ and × indicate different experimental conditions: The laser power is higher and the spectroscopic resolution lower for the □ points.

1. H||[001]

In Fig. 8 we present the experimental positions of the lines. As the field intensity increases, a new line appears at lower energy, the so-called A line. The B line splits into three components labeled B_1, B_2, and B_3 in order of increasing energy. When the slits are opened and the laser intensity is increased, a new line is also observed at higher energy (not seen in Fig. 7) labeled C_1. The B_1 and B_3 lines are mostly polarized perpendicular to [001], whereas A and B_2 lines are polarized parallel to [001].

2. H||[111]

B line splits into three components labeled B_1, B_2, and B_3. As the field intensity increases, three new lines appear: one at lower energy, labeled A, and two others at higher energy, labeled C_1 and C_2. The experimental positions of the lines are presented in Fig. 9. A, B_1, and B_3 are mostly polarized perpendicular to [111], whereas B_2 is most polarized parallel to [111].

3. H||[110]

B line also splits into three components labeled B_1, B_2, B_3, and as the field intensity increases three new lines appear, one at lower energy, labeled A, and the others at higher energy, labeled C_1 and C_2. When the slits are opened wide, another line labeled C_3, is detected. In Fig. 10 the experimental positions of the lines are presented.

B_2 line is mostly polarized parallel to [110], whereas B_3 and B_1 lines are mostly polarized perpendicular to [110]. In the three dimensions, all the lines remain thermalized together.

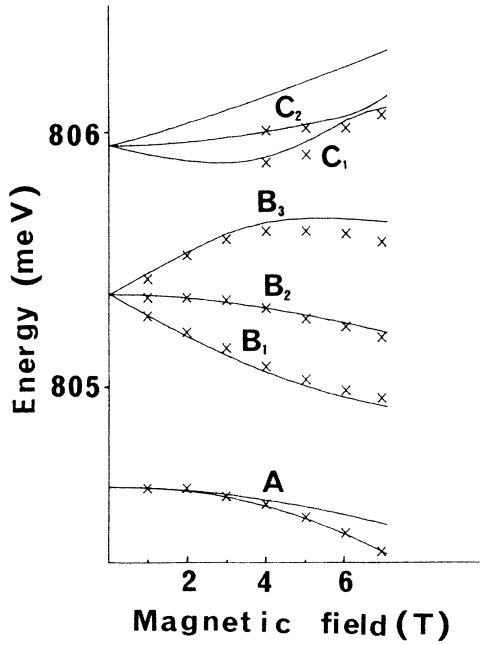

FIG. 9. Fan chart for H||[111]. The solid curves represent the theoretical positions of the transitions.

V. EXPERIMENTAL ANALYSIS

A. General discussion

The uniaxial stress and Zeeman experiments show that there are two excited levels near the initial level of the 805-meV transition, one at higher energy (initial level of the C lines, 805.6 meV), and the other at lower energy (initial level of the A lines, 804.7 meV).

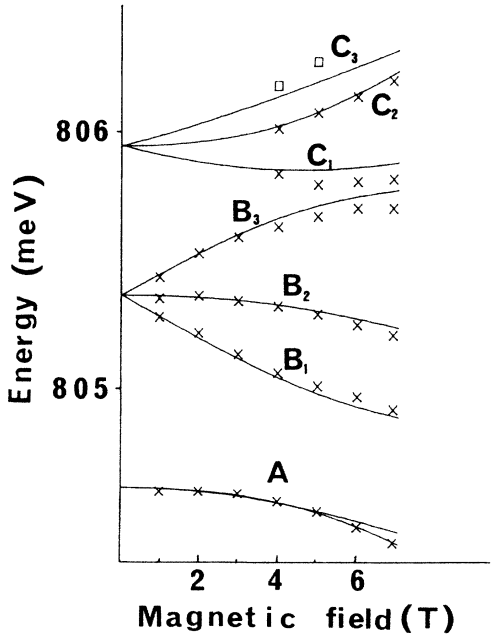

FIG. 10. H||[110]. The solid curves represent a fit based on (2), with the values of g_e, K, and L given in the text. □ and × indicate different experimental conditions: The laser power is higher and the spectroscopic resolution lower for the □ points.

The final state of the transition shows no splitting under a uniaxial stress or a magnetic field. Consequently this state should be a singlet. Since no orientational degeneracy is detected, the symmetry of the defect is T_d. This symmetry group has two representations of dimensionality one: Γ_1 and Γ_2. If we choose Γ_1 for the final state of the transition, the B line arises from a $\Gamma_5 \rightarrow \Gamma_1$ transition (the only one which is electric-dipole allowed). The following discussion is made in this scheme (a similar discussion can be made if B line is interpreted as a $\Gamma_4 \rightarrow \Gamma_2$ transition).

When stress is applied parallel to [001], the C line appears. The equivalent operator describing the effect of the tetragonal component of the stress belongs to $\Gamma_3(T_d)$, and it can induce a coupling between Γ_5 (transforming as $\Gamma_4+\Gamma_5$ in D_{2d}) and Γ_4 (transforming as $\Gamma_2+\Gamma_5$ in D_{2d}), then the only possibility for the C line is that it arises from a $\Gamma_4 \rightarrow \Gamma_1(T_d)$ transition (the $\Gamma_4 \rightarrow \Gamma_1$ transition is dipole-forbidden in T_d but is allowed when the stress is applied).

When stress is applied parallel to [111], the A line appears. As the equivalent operator describing the effect of the trigonal component of the stress belongs to $\Gamma_5(T_d)$, and the A line does not appear when P||[001], we have two possibilities.

(i) The A line arises from a $\Gamma_3 \rightarrow \Gamma_1(T_d)$ transition [$\Gamma_3(T_d)$ is reduced to Γ_3 in C_{3v}].

(ii) A line arises from a $\Gamma_1 \rightarrow \Gamma_1(T_d)$ transition [$\Gamma_1(T_d)$ is reduced to Γ_1 in C_{3v}].

But since the A line is polarized perpendicular to [111], we can rule out the latter possibility.

The associated energy-level scheme at zero field, with the deduced labels of symmetry is presented in Fig. 11. The $\Gamma_4+\Gamma_5+\Gamma_3$ states can be obtained from a $\Gamma_8 \otimes \Gamma_6$ product (or $\Gamma_8 \otimes \Gamma_7$), like the excited state of an exciton bound to an isoelectronic center. The ground state of the system is $^1A_1$. (As we have said the B line can also be interpreted as a $\Gamma_4 \rightarrow \Gamma_2$ transition, then the C line arises from a $\Gamma_5 \rightarrow \Gamma_2$ transition, the experiment can not rule out this possibility, but it has less physical meaning.) In the following section we have chosen the $\Gamma_8 \otimes \Gamma_7$ coupling, the reasons for this choice will be seen later (see Sec. VI).

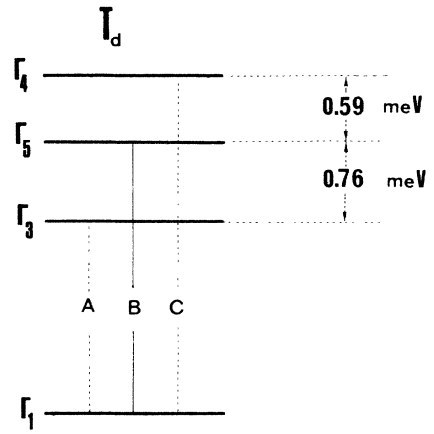

FIG. 11. Energy-level scheme of the 805-meV transition.

B. Uniaxial stress

The Γ_7 state (or Γ_6) does not split under an uniaxial stress, but the Γ_8 state does split. The effect of a uniaxial stress on the Γ_8 state can be described by the following operators for [001], [110], or [111] stress:

$$V_p^{[001]}=A_1PJ^2+BP(J_z^2-\tfrac{1}{3}J^2)\ ,$$

$$V_p^{[110]}=A_1PJ^2-\frac{BP}{2}(J_z^2-\tfrac{1}{3}J^2)+\frac{3CP}{2}(J_xJ_y+J_yJ_x)\ , \tag{1}$$

$$V_p^{[111]}=A_1PJ^2+CP(J_xJ_y+J_yJ_x)+\text{c.p.}\ ,$$

$$J\equiv\tfrac{3}{2}\ .$$

Using for the Γ_3, Γ_4, and Γ_5 levels the wave functions arising from a $\Gamma_7\otimes\Gamma_8$ coupling, which can be found in a standard table for the reduction of products of representations (the one used here was that of G. Koster and coworkers[4]), the diagonalization of Eq. (1) in the initial states of the transition can be easily done. The theoretical positions of the dipolar-allowed transitions are presented in Figs. 3, 4, and 5, together with the experimental positions of the lines. The best adjustment found between theory and experiment gives the following tetragonal (B), trigonal (D), and hydrostatic (A) coupling coefficients:

$$A=-0.011\ \text{meV/MPa}\ ,$$

$$B=0.04\ \text{meV/MPa}\ ,$$

$$C=0.028\ \text{meV/MPa}\ .$$

The polarization of the lines are also in agreement with the model. For example, in Fig. 12 we present the polarization spectra when $\mathbf{P}||[001]$. The C and B_2 lines are polarized perpendicular to [001], and the B_1 line is polarized parallel to [001]. The C and B_2 lines arise from a $\Gamma_5\rightarrow\Gamma_1$ transition in D_{2d}, whereas the B_1 line arises from a $\Gamma_4\rightarrow\Gamma_1$ transition in D_{2d}.

C. Zeeman effect

The Zeeman interaction in the initial state of the transition can be described in a very general way by an effective Hamiltonian perturbation of the following type:

$$h_{\text{eff}}=\mu_B g_e\mathbf{S}\cdot\mathbf{H}+\mu_B K\mathbf{J}\cdot\mathbf{H}+L\mu_B(J_x^3H_x+J_y^3H_y+J_z^3H_z)\ . \tag{2}$$

In this equation the first term represents the interaction within Γ_7 and the second and third terms the interaction within Γ_8. The best fit to the Zeeman data is found for the following g_e, K, and L values:

$$g_e=-0.55\ ,$$

$$K=1.1\ ,$$

$$L=0\ .$$

The theoretical positions of the dipole-allowed transitions are presented in Figs. 8, 9, and 10 together with the experimental position of the lines. In Fig. 13 we present the angular dependence of the lines under study at 6 T.

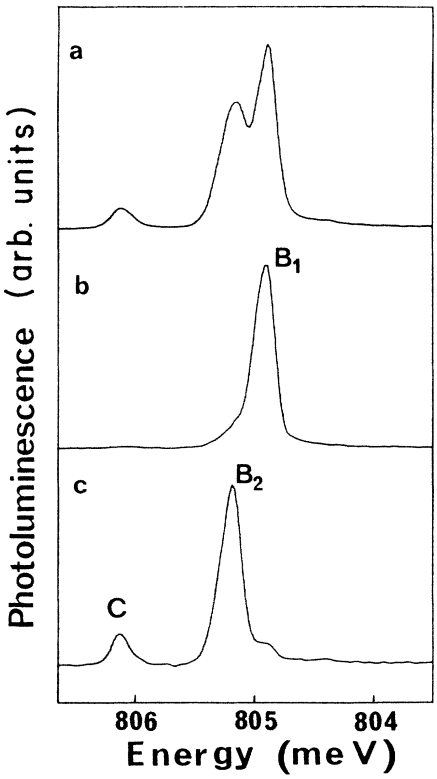

FIG. 12. Polarization spectra for the [001] stress ($P\sim100$ MPa). (a) Spectrum recorded without polarization; (b) spectrum recorded with $\mathbf{e}||[001]$; and (c) spectrum recorded with $\mathbf{e}\perp[001]$.

The magnetic field is rotated in a (110) plane. The solid curves are a fit based on the Hamiltonian Eq. (2), the points are the experimental positions of the lines; the line C_3 is only seen when the slits are wide open; its calculated intensity (see Sec. V D) is very weak.

Figure 14 shows the polarization spectra when

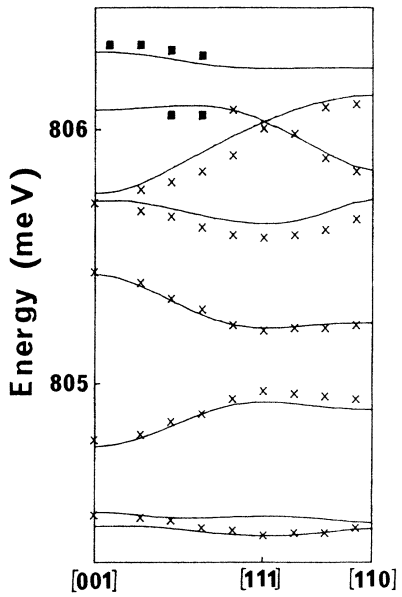

FIG. 13. Angular dependence of the lines upon rotation of the magnetic field in a (110) plane. The field intensity is 6 T.

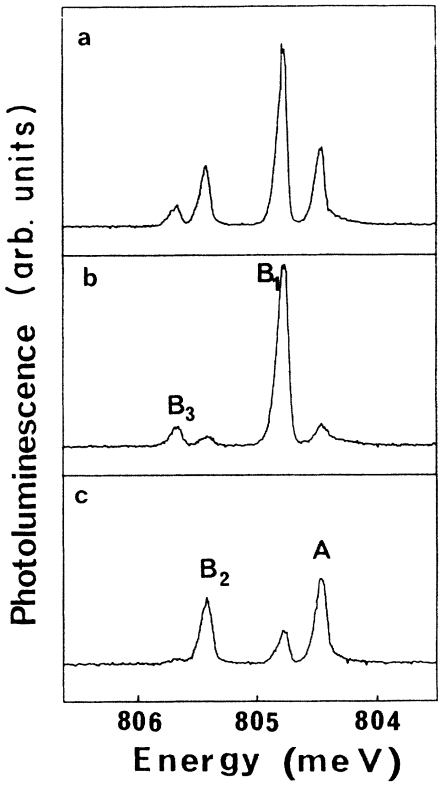

FIG. 14. Polarization spectra for H||[001] ($H=6$ T). The (b) and (c) spectra are normalized to B_1. (a) Spectrum recorded without polarization; (b) spectrum recorded with e⊥[001]; and (c) spectrum recorded with e||[001].

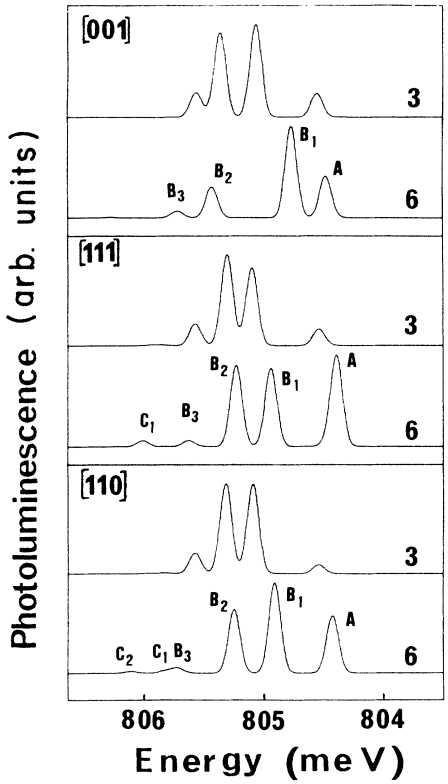

FIG. 15. Theoretical Zeeman spectra for a field intensity of 3 or 6 T.

H||[001]. According to the model A and B_2 lines arise from a $\Gamma_2 \rightarrow \Gamma_1$ transition in S_4, whereas B_1 and B_3 arise from a $\Gamma_3 \rightarrow \Gamma_1$ or $\Gamma_4 \rightarrow \Gamma_1$ transition in S_4, then A and B_2 lines should be polarized parallel to [001] and B_1 and B_3 perpendicular to [001]; they are indeed mostly polarized according to the model; the disagreement between theory and experiment could be attributed to some internal random stress existing in the sample, or to a small disorientation of the sample in the magnetic field.

D. Oscillator strengths

With the operators in Eqs. (1) and (2) we can calculate the mixing between the Γ_3 and Γ_5, and between the Γ_4 and Γ_5, wave functions induced by the uniaxial stress or the magnetic field; then the theoretical spectra can be obtained. As an example in Fig. 15, we present these theoretical spectra when the magnetic field is applied parallel to [001], [111], or [110], for a magnetic field of 3 or 6 T. The line shapes are taken as Gaussian of equal width, and a sample temperature of 4.5 K is assumed. This figure should be compared with the observed spectra shown in Fig. 7.

VI. DISCUSSION

The no-phonon line under study is at 805 meV, not far from the energy difference between the conduction band and the donor level of platinum (0.83 eV), this coincidence suggests that this transition is associated with the donor level (Pt^+/Pt^0) of platinum.

Platinum ($5d^9 6s^1$) is isoelectronic to nickel ($3d^9 4s^1$). The self-consistent calculations made by DeLeo and coworkers[5,6] for interstitial Ni show that it introduces two monoelectronic levels of e and t_2 symmetry in the band gap near the valence-band edge. The wave functions of these levels are delocalized, and the energy difference between them is very small, a similar behavior is expected for interstitial Pt. According to these authors the ground state of Ni^0 is $^1A_1(e^4 t_2^6)$, then the ground state of Pt^0 should also be $^1A_1$, as is the ground state of the detected transition. Then, we suggest that this transition is associated with interstitial Pt^0:

The final state of the transition is the ground state of interstitial Pt^0. The initial states of the transition arise from a $\Gamma_8 \otimes \Gamma_7$ (or $\Gamma_8 \otimes \Gamma_6$) product. The Γ_8 state could be related to the ground state of interstitial Pt, whereas the Γ_7 state could be related to the ground state of an electron bound to the Coulomb field of Pt^+.

By analogy to Ni, the energy difference between the configurations of Pt, $t_2^6 e^3$ and $t_2^5 e^4$, should be very small. The spin-orbit interaction transforms $t_2^6 e^3$ into Γ_8 and $t_2^5 e^4$ into $\Gamma_8 + \Gamma_7$. A detailed calculation of what is the ground state of interstitial Pt^+ is outside the scope of this paper, but since the intensity of the spin-orbit interaction of Pt is greater than that of Ni we suggest a Γ_8 state arising from the mixing of both configurations, moreover the K and L values obtained are very similar to the K and L

values of the shallow acceptor centers, which have delocalized wave functions as do the calculated wave functions of Ni^+.

The Coulomb field of Pt^+ can bind an electron. In the effective-mass approximation, the ground state of this electron is $1s$ $({}^2A_1+{}^2T_2+{}^2E)$ and the binding energy is 31 meV.[7] This level is split by the valley-orbit and spin-orbit interactions. Between the two well-characterized interstitial donors in silicon [Li and Mn (Refs. 8 and 9)] there is a striking difference: the ground state of Li is ${}^2E+{}^2T_2$, whereas that of Mn is ${}^2A_1$. The spin-orbit interaction transforms ${}^2A_1$ into Γ_6, ${}^2T_2$ into $\Gamma_8+\Gamma_7$, and ${}^2E$ into Γ_8. The g factor of $\Gamma_7({}^2T_2)$ alone is -0.66, very similar to the one found. It is this similarity which suggests that the ground state for the electron is $\Gamma_7({}^2T_2)$ and not $\Gamma_6({}^2A_1)$, which has a g value of 2. This suggested behavior (inversion of levels) is somehow similar to interstitial Li in silicon.

The exchange-interaction between the Γ_7 electron and the Γ_8 ground state of Pt^+ gives the initial states of the transition: $\Gamma_3+\Gamma_4+\Gamma_5$.

VII. SUMMARY

In this paper we have presented a photoluminescence study of Si:Pt. Two transitions are detected, which are related to two different centers. A detail study of one of them is presented. The experimental results of this latest transition are well interpreted in terms of a $\Gamma_3+\Gamma_5+\Gamma_4+\Gamma_1$ transition in T_d symmetry. The $\Gamma_3+\Gamma_5+\Gamma_4$ levels arise from a $\Gamma_8\otimes\Gamma_7$ product (very similar to the excited state of an exciton bound to an isoelectronic center). The energy of this transition suggests that it is related to the donor center of platinum in silicon. A suggestion of the possible nature of this transition is presented: a transition with a Pt^0 at an interstitial site.

ACKNOWLEDGMENT

The Laboratoire de Physique des Solides is "Laboratoire associé au Centre National de la Recherche Scientifique."

[1]M. Pugnet, J. Barbolla, J. C. Brabant, F. Saint-Yves, and M. Brousseau, Phys. Status Solidi A **35**, 533 (1976).

[2]H. H. Woodbury and G. W. Ludwing, Phys. Rev. **126**, 466 (1962).

[3]J. C. M. Henning and E. C. J. Egelmeers, Phys. Rev. B **27**, 4002 (1983).

[4]G. F. Koster, J. O. Dimmock, R. G. Wheeler, and H. Statz, *Properties of the Thirty-Two Point Groups* (MIT, Cambridge, Mass., 1963).

[5]G. G. Deleo, G. D. Watkins, and W. B. Fowler, Phys. Rev. B **25**, 4962 (1982).

[6]G. G. Deleo, G. D. Watkins, and W. B. Fowler, Phys. Rev. B **25**, 4972 (1982).

[7]R. A. Faulkner, Phys. Rev. **184**, 713 (1969).

[8]R. L. Aggarwal, P. Fisher, V. Mourzine, and A. K. Ramdas, Phys. Rev. **138**, A882 (1965).

[9]L. T. Ho and A. K. Ramdos, Phys. Rev. B **5**, 462 (1972).